Science of the Total Environment 803 (2022) 150002

Contents lists available at ScienceDirect

Science of the Total Environment

journal homepage: www.elsevier.com/locate/scitotenv

First-year sea ice leads to an increase in dimethyl sulfide-induced particle formation in the Antarctic Peninsula

Eunho Jang [a,b], Ki-Tae Park [a,b,*], Young Jun Yoon [a], Kitae Kim [a,b], Yeontae Gim [a], Hyun Young Chung [a,b], Kitack Lee [c], Jinhee Choi [a], Jiyeon Park [a], Sang-Jong Park [a], Ja-Ho Koo [d], Rafael P. Fernandez [e], Alfonso Saiz-Lopez [f]

[a] Korea Polar Research Institute, Incheon, South Korea
[b] University of Science and Technology, Daejeon, South Korea
[c] Department of Environmental Science and Engineering, Pohang University of Science and Technology, Pohang, South Korea
[d] Department of Atmospheric Sciences, Yonsei University, Seoul, South Korea
[e] Institute for Interdisciplinary Science (ICB), National Research Council (CONICET), FCEN-UNCuyo, Mendoza, Argentina
[f] Department of Atmospheric Chemistry and Climate, Institute of Physical Chemistry Rocasolano, CSIC, Madrid, Spain

HIGHLIGHTS

- DMS, its oxidation products, and aerosols were measured in the Antarctic atmosphere.
- Emission and oxidation of DMS were highly source region dependent.
- DMS emission was associated with the abundance of DMS producers in source regions.
- DMS oxidation was primarily affected by atmospheric BrO levels in source regions.
- First-year sea ice accelerates particle formation by acting as DMS and BrO source.

GRAPHICAL ABSTRACT

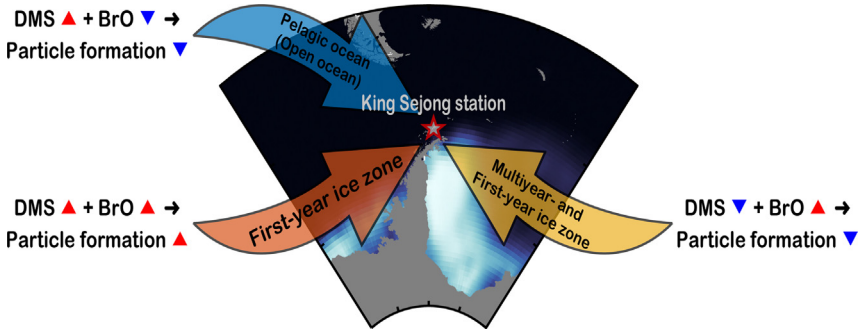

ARTICLE INFO

Article history:
Received 24 June 2021
Received in revised form 17 August 2021
Accepted 25 August 2021
Available online 31 August 2021

Editor: Pingqing Fu

Keywords:
Dimethyl sulfide
Sulfurous particles
New particle formation
Bromine monoxide
First-Year Sea ice
Antarctic peninsula

ABSTRACT

Dimethyl sulfide (DMS) produced by marine algae represents the largest natural emission of sulfur to the atmosphere. The oxidation of DMS is a key process affecting new particle formation that contributes to the radiative forcing of the Earth. In this study, atmospheric DMS and its major oxidation products (methanesulfonic acid, MSA; non-sea-salt sulfate, nss-SO_4^{2-}) and particle size distributions were measured at King Sejong station located in the Antarctic Peninsula during the austral spring–summer period in 2018–2020. The observatory was surrounded by open ocean and first-year and multi-year sea ice. Importantly, oceanic emissions and atmospheric oxidation of DMS showed distinct differences depending on source regions. A high mixing ratio of atmospheric DMS was observed when air masses were influenced by the open ocean and first-year sea ice due to the abundance of DMS producers such as pelagic *phaeocystis* and ice algae. However, the concentrations of MSA and nss-SO_4^{2-} were distinctively increased for air masses originating from first-year sea ice as compared to those originating from the open ocean and multi-year sea ice, suggesting additional influences from the source regions of atmospheric oxidants. Heterogeneous chemical processes that actively occur over first-year sea ice tend to accelerate the release of bromine monoxide (BrO), which is the most efficient DMS oxidant in Antarctica. Model-estimates for surface BrO confirmed that high BrO mixing ratios were closely associated with first-year sea ice, thus enhancing DMS oxidation. Consequently, the concentration of newly formed particles originated from first-year sea ice, which was a strong source area for both DMS and BrO was greater than from open ocean

* Corresponding author at: Korea Polar Research Institute, Incheon, South Korea.
E-mail address: ktpark@kopri.re.kr (K.-T. Park).

https://doi.org/10.1016/j.scitotenv.2021.150002

(high DMS but low BrO). These results indicate that first-year sea ice plays an important yet overlooked role in DMS-induced new particle formation in polar environments, where warming-induced sea ice changes are pronounced.

1. Introduction

Dimethyl sulfide (DMS) is mostly of a marine origin and is the largest source of natural sulfur to the atmosphere (Simó, 2001). Biogenic DMS is produced by the enzymatic cleavage of dimethylsulfoniopropionate (DMSP) (Stefels et al., 2007). Marine algae metabolize DMSP as a defense mechanism that acts as an osmolyte, cryoprotectant, antioxidant, and predator suppressor (Kirst et al., 1991; Strom et al., 2003; Sunda et al., 2002). DMS production in marine environments is closely linked with both the biomass and taxonomic composition of marine algae because the production of algal DMSP and its degradation into DMS are highly species-specific (Keller et al., 1989; Park et al., 2018; Park et al., 2014). The Southern Ocean has a greater potential for DMS and DMSP production during the austral spring–summer period, largely owing to a massive bloom of strong DMS producers (Curran and Jones, 2000; Lana et al., 2011). Thus, sea surface DMS concentrations in the Southern Ocean are estimated to be the highest on the globe, with mean values of >5 nM during the austral spring-summer period (Jarníková et al., 2018; Lana et al., 2011).

Airborne DMS is oxidized into other sulfur compounds, including sulfur dioxide (SO_2), methanesulfonic acid (MSA), and hydroperoxymethyl thioformate (HPMTF), through radical-initiated reactions with atmospheric oxidants (Chen et al., 2018; von Glasow and Crutzen, 2004; Veres et al., 2020). Several oxidants, including hydroxyl radical (OH), nitrate radical (NO_3), and halogen radicals (such as bromine monoxide and chlorine), are involved in atmospheric DMS oxidation processes (Barnes et al., 2006). Importantly, the relative contribution of these key atmospheric oxidants to the DMS oxidation process shows latitudinal and seasonal variations (Boucher et al., 2003). Gas-phase sulfuric acid (H_2SO_4), a more oxidized form of SO_2, and MSA can trigger new particle formation via homogeneous and heterogeneous nucleation with H_2O and N compounds. DMS-derived sulfurous particles can also induce particle growth by condensing with pre-existing particles due to their low volatility (Hodshire et al., 2018; Holmes, 2007; Veres et al., 2020). The formation and growth of these sulfurous aerosol particles can then increase the cloud condensation nuclei (CCN) concentration due to their high hygroscopicity, thereby affecting the microphysical properties of clouds (Boucher and Lohmann, 1995; Charlson et al., 1987; Mahajan et al., 2015; Park et al., 2021; Sanchez et al., 2018).

Marine aerosols are major components that modulate radiative forcing on climate systems in the remote marine atmosphere (Brooks and Thornton, 2018). The major components of marine aerosols are primary sea spray aerosols emitted directly from the sea surface microlayer and secondary marine aerosols formed via chemical oxidation processes of volatile organic compounds (Brooks and Thornton, 2018; Piller-Little and Guzman, 2018). Among the climate forcers, aerosols and their precursors contribute to a significant portion of the negative radiative forcing by scattering downward solar radiation (direct effect) and modifying the microphysical properties of clouds (indirect effect) (Carslaw et al., 2013; Haywood and Boucher, 2000). The physiochemical properties of marine aerosols are tightly connected with the seasonal progression of marine biota (O'Dowd et al., 2004). Particularly, biogenic DMS can play major roles in the formation and growth of aerosol particles during the productive period in polar regions where the existing condensation sink is small (Chang et al., 2011; Jang et al., 2019; Leaitch et al., 2013; Park et al., 2017).

Considering that the Antarctic Peninsula is the one of the fastest-warming areas on Earth (Tuckett et al., 2019), severe environmental changes (e.g., sea surface warming, stratification, and sea ice retreat) can alter the sea ice biogeochemistry and marine ecosystem, which are closely linked with DMS-induced particle formation in the pristine marine atmosphere (Browse et al., 2014; Dall'Osto et al., 2017a; Yan et al., 2020a). However, the quantitative association of DMS-induced particle formation with algal assemblages and sea-ice properties remains poorly studied in the Southern Ocean. Moreover, the ocean–cryosphere–atmosphere interactions that affect marine aerosols remain largely unknown due to their complexity and geographical characteristics (i.e., low accessibility and harsh environment) that limit research in Antarctica.

In this study, atmospheric DMS, MSA, and non-sea salt sulfate (nss-SO_4^{2-}) as well as aerosol size distributions were measured at the King Sejong station (62.2° S, 58.8° W) in the Antarctic Peninsula during the austral spring–summer period from 2018 to 2020. We also analyzed the air mass transport history, satellite-based estimates of environmental parameters (including chlorophyll and DMSP concentrations, taxonomic compositions of phytoplankton, and sea ice properties), and model-estimates for reactive halogen species to determine the main source-appointment regions that dominantly influence DMS oxidation. Ultimately, this study provides in-situ measurements of physiochemical properties of aerosols, satellite- and model-estimates for multiple environmental variables to discuss source region-dependent oceanic DMS emissions and atmospheric DMS oxidation, and DMS-induced particle formation process in the Antarctic environment.

2. Materials and methods

2.1. Atmospheric measurements

King Sejong station (62.2° S, 58.8° W) is located in the Antarctic Peninsula, surrounded by open ocean and first-year and multi-year sea ice (Fig. 1a). The atmospheric observatory is approximately 10 m above sea level and 400 m northwest of the main facilities of King Sejong station. Concurrent observations of atmospheric DMS mixing ratios, aerosol size distributions, and meteorological parameters were conducted from December 2018 to April 2019 and from November 2019 to February 2020.

The atmospheric DMS mixing ratios were measured at 20 min to 1 h intervals using a DMS analyzer consisting of a custom-made DMS trapping and thermal desorption system, a gas chromatograph (7890B GC, Agilent Technologies, Inc.), and a pulsed flame photometric detector (PFPD 5383, OI Analytical, Inc.) (Jang et al., 2016). To measure the chemical properties of the aerosol particles, a high-volume air sampler (HV-1000R, Sibata Scientific Technology, Inc.), equipped with a $PM_{2.5}$ impactor (collecting particles <2.5 μm in aerodynamic diameter), was used to collect aerosol particles at 1–3-day intervals from January to February 2019 and from December 2019 to January 2020. Aerosol particles were collected on pre-baked quartz filters at a flow rate of 1000 L min^{-1}. A wind sector controller was used to suspend the air sampling under pollution sector conditions (i.e., when the wind direction was in the range of 355–55° or at wind speeds <2 m s^{-1}) to minimize the influence of local emissions from the power generators and incinerator (Kim et al., 2019a; Kim et al., 2017). To measure the major ions, the 47 mm (diameter) quartz filter was collected, and the major ions in the disk filter were concentrated into 20 mL of Milli-Q water. The concentrations of the major ions, including Na^+, SO_4^{2-}, and MSA, were detected by ion chromatography (Dionex AQUION fitted with a CS12A IonPac

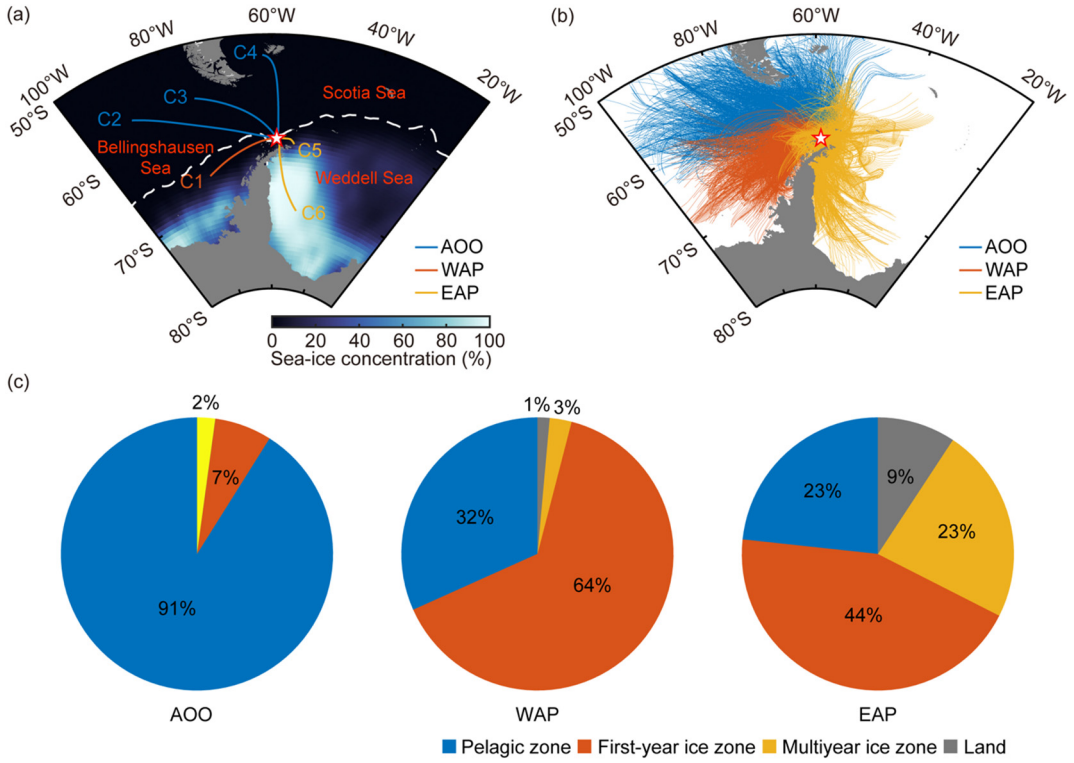

Fig. 1. (a) Mean sea ice concentration overlain with the six clusters of the 2-day air mass back trajectory (C1: western Antarctic Peninsula, WAP; C2–C4: Antarctic open ocean, AOO; C5 and C6: eastern Antarctic Peninsula, EAP) during the study period (December 2018 to April 2019 and November 2019 to February 2020). The white dashed line represents the maximum sea ice extent observed in August 2018 and 2019. (b) 2-day air mass back trajectories collected at hourly intervals during the study period. Blue, orange, and yellow lines denote the trajectories categorized into three groups: AOO, WAP, and EAP, respectively. The red star symbol shows the location of the observation site, King Sejong station (62.2°S, 58.8°W). (c) Percentage of air mass retention time over the four terrains, including the pelagic zone, first-year ice zone, multi-year ice zone, and land in the AOO, WAP, and EAP.

column for cations and Dionex ICS-1100 fitted with an AS19 column for anions, Thermo Fisher Scientific, Inc.). The concentration of nss-SO_4^{2-} was calculated based on the following equation: [nss-SO_4^{2-}] = $[SO_4^{2-}]_{total} - [Na^+] \times 0.252$, where 0.252 is the ratio of SO_4^{2-} to Na^+ in seawater (Keene et al., 1989).

The aerosol size distributions between 10 and 300 nm of mobility equivalent diameter were measured at 3 min intervals using a scanning mobility particle sizer (SMPS), consisting of a condensation particle counter (CPC3772, TSI, Inc.) and a differential mobility analyzer (LDMA 4210, HCT, Inc.). The black carbon concentrations were measured at 10 min intervals using two aethalometers (AE16 in 2019 and AE33 in 2020; Magee Scientific, Inc.) from aerosol absorption coefficients at a frequency of 880 nm. The datasets from the SMPS that met the conditions of the pollution sector or those with a black carbon concentration of >50 ng m^{-3} were excluded from the analysis to avoid local influences.

2.2. Air mass origin classification

The hybrid single-particle Lagrangian integrated trajectory (HYSPLIT) model and global meteorological archives obtained from the global data assimilation system (GDAS) were used to generate 2-day air mass back trajectories (Stein et al., 2015). The backward time of 2-day was selected given the DMS loss rates of 38–68% day^{-1} in the polar atmosphere (Sharma et al., 1999). To identify the main air mass transport pathway, cluster analysis was conducted using 2-day air mass back trajectories during the study period. The optimum number of clusters was determined from the change in total spatial variations (Stein et al., 2015).

The daily geographical data including sea ice, ocean, and land were obtained from the National Snow and Ice Data Center (NSIDC). In this study, we defined the domains of pelagic, first-year ice, and multi-year ice zones based on the following criteria:

(1) pelagic zone: open ocean area that does not include first-year or multi-year ice zones.
(2) first-year ice zone: the area between the maximum (austral winter; August) and minimum (at measured day) seasonal ice limit, plus the transition area where the sea ice concentration is <80% (Strong and Rigor, 2013).
(3) multi-year ice zone: pack-ice area where the sea ice concentration is >80% (Strong and Rigor, 2013).

Then, the results for the air mass back trajectory analysis and geographical information were combined to elucidate the potential source region of air masses reaching the observation site (Choi et al., 2019; Park et al., 2020). For each 2-day air mass back trajectory, the number of trajectory time points (n = 1–48) assigned to one of three domains was divided by the total trajectory time points (n = 48) to calculate the percentage of the air mass retention time over the pelagic, first-year ice, and multi-year ice zones.

2.3. Satellite- and model-estimates for environmental variables

The 8-day composite products of the chlorophyll concentration derived from the moderate resolution imaging spectroradiometer on the Aqua satellite (MODIS-Aqua) were used to indicate phytoplankton biomass. The 8-day mean total DMSP concentrations (DMSPt) were retrieved from the DMSPt algorithm (Galí et al., 2015). The monthly climatology maps with dominant frequencies of the five phytoplankton groups, including nanoeukaryotes, *prochlorococcus*, *synechococcus*, diatoms, and *phaeocystis* were obtained from the PHYSAT algorithm

(Alvain et al., 2008). The surface mixing ratios of the reactive halogen species including bromine monoxide (BrO) and iodine monoxide (IO) were obtained from the halogen version of the Community Atmosphere Model with Chemistry (CAM-Chem) model (Fernandez et al., 2019).

3. Results

3.1. Classification of air mass origin

Six clusters of air masses were obtained from 5016 hourly air mass back trajectories and were reclassified into three groups representing the Antarctic open ocean (AOO; C2, C3, and C4), western Antarctic Peninsula (WAP; C1), and eastern Antarctic Peninsula (EAP; C5 and C6) (Fig. 1a and b). The air masses assigned for AOO ($n = 1983$), WAP ($n = 1675$), and EAP ($n = 1358$) showed different origins: AOO mostly originated from the open ocean (pelagic zone 91%, first-year ice zone 7%, and multi-year ice zone 2%), while WAP and EAP were characterized by longer air mass exposures to ice-related areas (pelagic zone 32%, first-year ice zone 64%, and multi-year ice zone 3% for the WAP; pelagic zone 23%, first-year ice zone 44%, and multi-year ice zone 23% for the EAP) (Fig. 1c). The WAP and EAP were most exposed to the first-year ice zone during the study period; the WAP had the highest exposure to the first-year ice zone, at 9.1- and 1.5-fold greater than that of the AOO and EAP, respectively. Air masses assigned for the EAP had the highest air mass retention time over the multi-year ice zone, 11.5- and 7.7-fold greater than that of the AOO and WAP, respectively. Thus, the AOO, WAP, and EAP regions were considered to represent the zones of being pelagic dominant, being the first-year ice dominant, and being the first-year and multi-year ice dominant, respectively.

3.2. In-situ measurements for atmospheric DMS, its oxidative products, and aerosol particles

The hourly DMS mixing ratios ranged from 1.0 to 593.2 pptv, with a mean value of 43.7 ± 36.7 pptv (Fig. 2a). These temporal variations were similar to those observed at other Antarctic sites, including the Palmer station (64.8°S, 64.1°W; 6–595 pptv) (Berresheim et al., 1998) and the Halley station (75.6°S, 26.6°W; 5–286 pptv) (Read et al., 2008). As confirmed in other studies, the short-term variability of atmospheric DMS levels is closely associated with the strength of oceanic DMS sources and meteorological conditions (e.g., Berresheim et al., 1998; Jang et al., 2021; Mungall et al., 2016; Park et al., 2013; Read et al., 2008). The concentrations of MSA and nss-SO_4^{2-} varied from 44.6–196.9 and from 85.5–558.8 ng m^{-3}, respectively (Fig. 2b), with corresponding mean values of 96.3 ± 32.8 and 225.5 ± 97.4 ng m^{-3}. Temporal variations in MSA and nss-SO_4^{2-} were comparable to previous observation at the King Sejong station (73.1 ± 58.7 ng m^{-3} and 140.1 ± 69.7 ng m^{-3}, respectively) (Hong et al., 2020) and Marambio station (64.2°S, 56.7°W; monthly mean variations of 19–78 and 133–430 ng m^{-3}, respectively) (Asmi et al., 2018). Sulfate particles in the atmosphere have multiple sources including sea salt, biogenic DMS, and anthropogenic SO_2, while atmospheric MSA in the remote

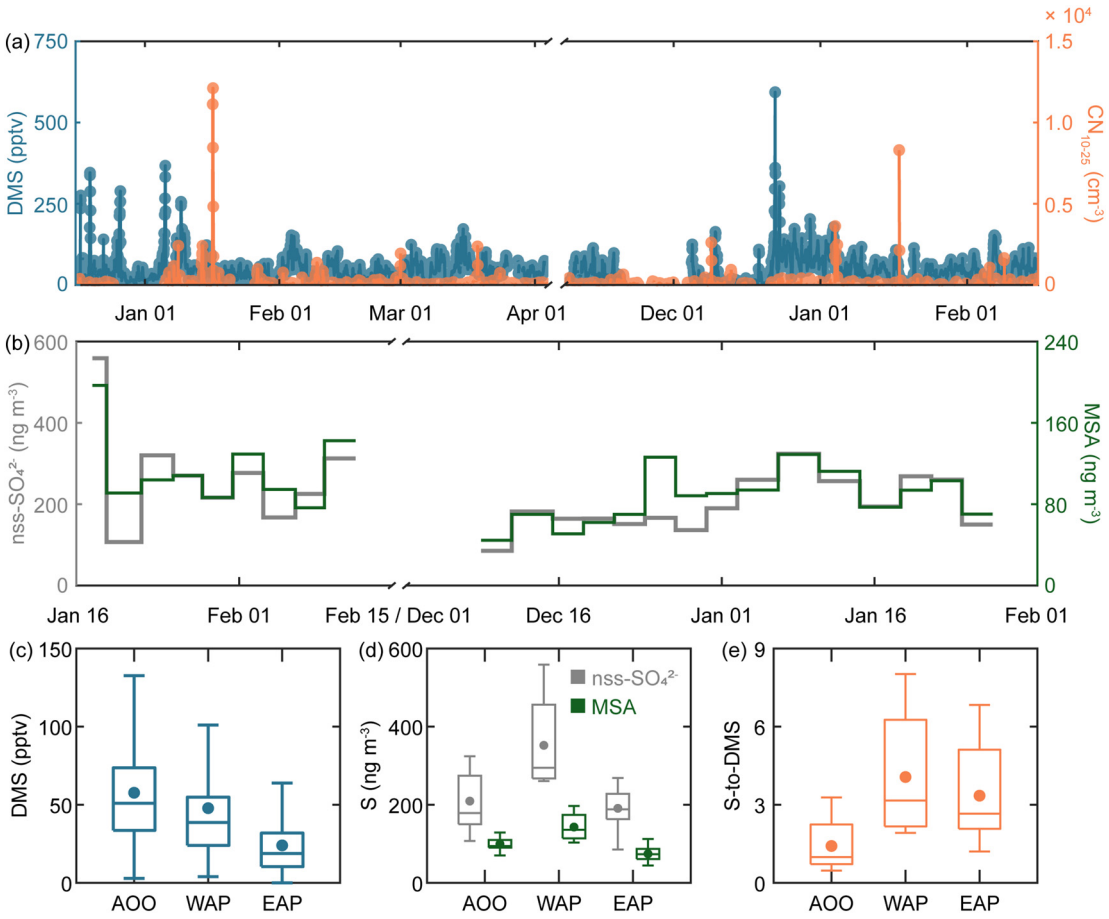

Fig. 2. (a) Mixing ratios of the hourly mean atmospheric DMS (blue circles and line) and the number concentration of the hourly mean newly formed particles (CN_{10-25}; 10 to 25 nm in diameter) (orange circles and line). (b) Concentrations of non-sea salt SO_4^{2-} (nss-SO_4^{2-}) (grey line) and MSA (green line) during the study period. Box plots for the (c) atmospheric DMS mixing ratios, (d) concentrations of sulfur compounds (S; nss-SO_4^{2-} and MSA), and (e) sulfur compounds (the sum of nss-SO_4^{2-} and MSA)-to-DMS mixing ratios (S-to-DMS) assigned for the AOO, WAP, and EAP. In the box plots, the solid middle lines, circles, box edges, and whiskers represent the median, mean, 25th, and 75th percentile, and Q1 and Q3, respectively.

marine boundary layer originated only from the oxidation of DMS (Chen et al., 2018). Here, positive correlation between the MSA and nss-SO_4^{2-} ($r^2 = 0.71$, $n = 24$) indicated that both species were mostly formed via biogenic DMS oxidation (Fig. 3). All of the in-situ measurements for the atmospheric DMS and its oxidative products (i.e., MSA and nss-SO_4^{2-}) showed similar temporal variations to those of previous studies conducted at other Antarctic sites during the spring–summer period (e.g., Berresheim et al., 1998; Read et al., 2008; Asmi et al., 2018).

All atmospheric DMS mixing ratios and the concentrations of MSA and nss-SO_4^{2-} in the AOO, WAP, and EAP showed notable differences (Fig. 2c and d). The highest mean atmospheric DMS mixing ratio originated from the AOO (57.7 ± 36.9 pptv, $n = 1742$), comparable with that from the WAP (47.8 ± 41.7 pptv, $n = 1185$) (Fig. 2c). Air masses originating from the EAP showed the lowest mean atmospheric DMS mixing ratios (24.0 ± 19.8 pptv, $n = 1493$) (Fig. 2c). In contrast, the concentrations of MSA and nss-SO_4^{2-} were the highest for air masses from the WAP (142.9 ± 39.5 and 352.2 ± 139.4 ng m^{-3} ($n = 4$), respectively), followed by those from the AOO (99.6 ± 17.9 and 209.4 ± 78.0 ng m^{-3}, ($n = 10$), respectively) and EAP (74.4 ± 20.0 and 190.9 ± 54.2 ng m^{-3}, ($n = 10$), respectively) (Fig. 2d). Consequently, the biogenic sulfurous particles (sum of nss-SO_4^{2-} and MSA)-to-DMS ratios, which can imply the conversion efficiency of gaseous DMS into sulfurous particles, were more than two-fold higher in the WAP (4.1 ± 2.8) and EAP (3.3 ± 1.9) than those in the AOO (1.4 ± 1.0) (Fig. 2e). In a previous study carried out at the same location during the austral spring–summer period in 2013–2014, remarkably higher concentrations of MSA and nss-SO_4^{2-} were also detected in the $PM_{2.5}$ and PM_{10} samples for air masses originated from the western part of the Antarctic Peninsula (Hong et al., 2020). Further, recent shipboard observations in the pelagic Southern Ocean (covering 40°–76°S, 170°E–110°W) reported extremely low biogenic sulfurous particles-to-DMS (ranging from 0.012–0.33 ratios in February and March 2018 (Yan et al., 2020b). The MSA-to-DMS ratio measured at the Halley station (approximately 0.63 in 2004 and 0.24 in 2005) (Read et al., 2008), located in coastal Antarctica, was slightly lower than that of our study, but ten-fold higher than that in the pelagic Southern Ocean, as reported by Yan et al. (2020b).

The nucleation mode particle through the gas-to-particle conversion is defined as a particle <25 nm in diameter (Kerminen et al., 2018). In this study, the number concentrations of the aerosol particles in the range of 10–25 nm ($CN_{10–25}$) were used as an indicator of newly formed aerosol particles. Considerable short-term variability (~10 to $>10^4$ cm^{-3}) with a mean value of 128 ± 476 cm^{-3} was observed during the study period (Fig. 2a). The highest mean $CN_{10–25}$ was detected in the WAP (177 ± 777 cm^{-3}, $n = 779$), followed by the EAP (131 ± 287 cm^{-3}, $n = 892$) and the AOO (73 ± 74 cm^{-3}, $n = 767$) (Figs. 4f and S1). Notably, the differences in nano-size particles depending on air mass origin are consistent with the results of recent studies which show a higher frequency of new particle formation events for ice-influenced air masses in polar regions (Brean et al., 2021; Dall'Osto et al., 2017b; Jokinen et al., 2018; Lachlan-Cope et al., 2020).

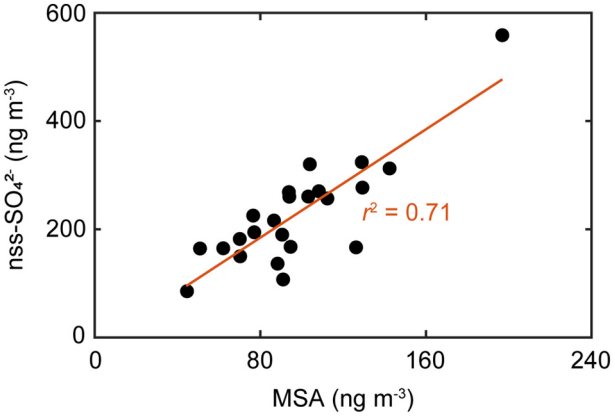

Fig. 3. Linear regression plot between the concentrations of MSA and nss-SO_4^{2-} during the study period. The red solid line indicates the best fit.

3.3. Environmental parameters related to the emissions and oxidation of DMS

Trajectory frequencies were calculated from the number of trajectory time points in each grid cell (0.5° resolution) divided by the total number of trajectories (Rolph et al., 2017). We limited our analysis to areas with trajectory frequencies of >2% to minimize the analytical bias caused by the grid cells with low trajectory frequencies when calculating the satellite-and model-estimates for the AOO, WAP, and EAP regions (Fig. S2). An intensive phytoplankton bloom was observed near the west coast of the Antarctic Peninsula and Scotia Sea (Fig. S3). Thus, the 8-day mean sea surface chlorophyll concentration was the highest in the EAP (0.40 ± 0.20 mg m^{-3}), followed by the WAP (0.35 ± 0.10 mg m^{-3}) and AOO (0.29 ± 0.10 mg m^{-3}) (Figs. 4a and S3a). The DMSP-to-chlorophyll ratios had notable differences between the three groups; AOO had the highest ratio (111.4 ± 35.5 mmol g^{-1}), followed by the WAP (87.6 ± 22.0 mmol g^{-1}) and EAP (72.1 ± 13.8 mmol g^{-1}) (Figs. 4b and S3b). Similar to the spatial patterns of the DMSP-to-chlorophyll ratio, the relative dominance of *phaeocystis* in the three regions had the following order: AOO (36.7 ± 18.1%), WAP (16.2 ± 12.5%), and EAP (10.2 ± 3.6%); however, that of the diatoms showed the opposite trend (11.2 ± 10.5, 22.5 ± 12.8, and 27.6 ± 15.0% for the AOO, WAP, and EAP, respectively) (Figs. 4c and S3c). The monthly mean surface BrO mixing ratio, as estimated by the CAM-Chem model, was highest during the austral spring period (0.9–2.0 pptv from September–November); the lowest mixing ratios occurred during the austral winter period, with monthly mean values of <0.1 pptv near the Antarctic Peninsula (50°–80° S, 20°–100° W) (Fig. S4a). The surface BrO mixing ratios were the highest in the WAP (0.67 ± 0.36 pptv), followed by the EAP (0.43 ± 0.13 pptv) and AOO (0.18 ± 0.10 pptv) during the study period (Fig. 4d). Year-round field observation of BrO at the Halley station represented similar seasonal variations with distinct short-term (< few hours) variations depending on air mass origin (Saiz-Lopez et al., 2007).

4. Discussion

4.1. Oceanic DMS emissions depending on source regions

Phaeocystis (DMSP-rich) and diatoms (DMSP-poor), which have opposite DMS and DMSP productivity, are major phytoplankton groups and are competitively dominant in the pelagic Southern Ocean (Arrigo et al., 2010). Thus, the dominance of DMSP-rich *phaeocystis* and resulting higher DMSP-to-chlorophyll ratio in the AOO and WAP could contribute to an increase in atmospheric DMS in the air masses that originate from these areas (Fig. 3b and c). Together, the larger expanse of first-year sea ice in the WAP could also contribute to the release of biogenic DMS into the atmosphere during the austral spring–summer period. Because an intensive ice algae bloom, which was frequently observed in the first-year sea ice, can serve as a significant source of atmospheric DMS (Koga et al., 2014; Levasseur, 2013; Trevena and Jones, 2006). In contrast, the lower atmospheric DMS level in the EAP was possibly associated with the relatively higher dominance of DMSP-poor diatoms and longer retention time of the air mass over the multi-year sea ice and land areas, which released less DMS, despite the highest mean chlorophyll concentration (Fig. 4a–3c). Consequently, the growth of strong DMS producers and the passage of air masses over the productive sites largely controlled the atmospheric DMS mixing ratios measured in the Antarctic Peninsula.

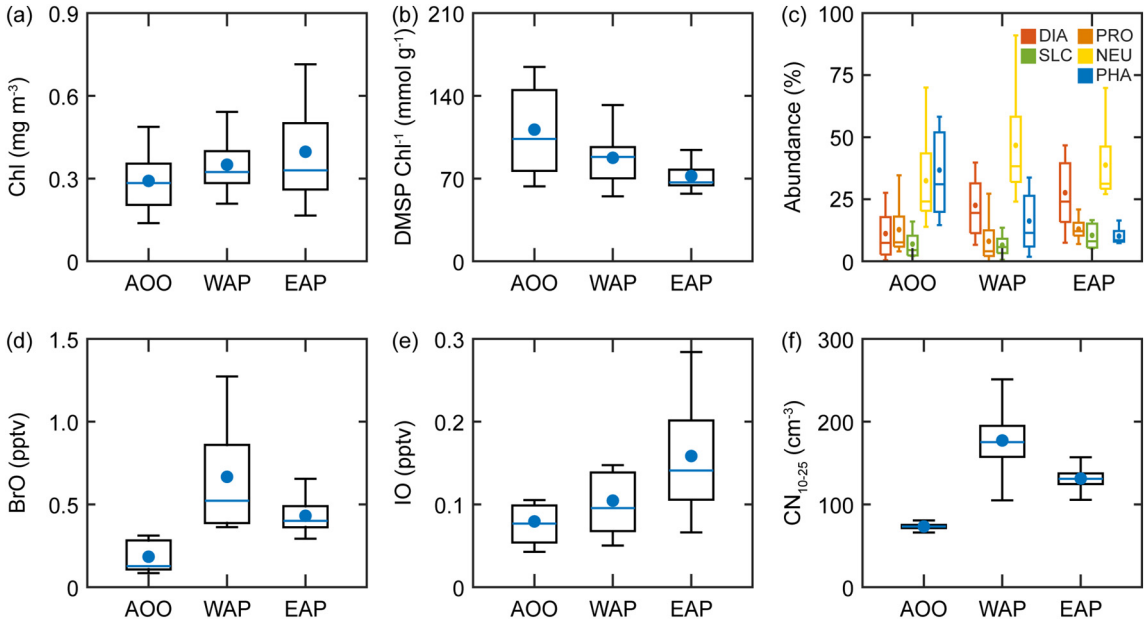

Fig. 4. Box plots for the (a) chlorophyll concentration, (b) DMSP-to-chlorophyll ratio, and (c) dominant phytoplankton groups including diatoms (DIA), prochlorococcus (PRO), synechococcus (SLC), nanoeukaryotes (NEU), and *phaeocystis* (PHA), (d) surface BrO mixing ratios, and (e) surface IO mixing ratios. (f) Bootstrapping estimation for the number concentration of newly formed particles (CN_{10-25}) for the AOO, WAP, and EAP during the study period. In the box plots, the solid middle lines, circles, box edges, and whiskers represent the median, mean, 25th, and 75th percentile, and Q1 and Q3, respectively.

4.2. Atmospheric DMS oxidation depending on source regions

Atmospheric DMS oxidation is largely controlled by the key oxidants, including OH, NO_3, and BrO (Barnes et al., 2006). Typically, the roles of OH and NO_3 in the Antarctic are relatively insignificant compared with tropical and temperate regions, owing to lower water vapor and UV radiation, as well as lower local anthropogenic emissions of nitrogen oxides (NO_x) (Chen et al., 2018). In contrast, reactive halogen species (containing chlorine, bromine, or iodine) significantly contribute to atmospheric oxidation processes in remote polar environments (Saiz-Lopez and von Glasow, 2012). Recent studies revealed unique natural processes, such as heterogeneous reactions of inorganic halide, halide fractionation in aerosolized seawater droplets, and photochemical decomposition of biogenic halocarbons, that affect the supply of reactive halogen species to the polar marine boundary layer (Guzman et al., 2012; Hughes et al., 2012; Lieb-Lappen and Obbard, 2015; Piller-Little et al., 2013; Pratt, 2019). Among these species, BrO is a well-known oxidant involving 50–60% DMS oxidation in the Antarctic boundary layer (Breider et al., 2010; von Glasow and Crutzen, 2004; Read et al., 2008). Importantly, BrO at sub-ppt levels in the marine boundary layer can have a significant impact on DMS oxidation at high latitudes (Boucher et al., 2003). As the lifetime of BrO in the boundary layer is less than 2 h, atmospheric levels of BrO are strongly influenced by the air mass origin (Saiz-Lopez et al., 2007). The surface BrO mixing ratios in the WAP and EAP were 3.7- and 2.3-fold higher than that in the AOO during the study period (Fig. 4d). High surface BrO mixing ratios were particularly consistent with the first-year sea ice (Figs. 1a and S5a). This is because the release of reactive halogen species is strongly activated by photochemical reactions and heterogeneous recycling that occur in the frost flower, brine channels, and snow-covered saline ice (Lieb-Lappen and Obbard, 2015; Saiz-Lopez et al., 2008; Simpson et al., 2007; Yang et al., 2008). Heterogeneous recycling of inorganic bromine species leads to the releases of more gas-phase Br_2 from the icy surface (i.e., the so-called bromine explosion) (Simpson et al., 2007). Then, the gas-phase Br_2 rapidly undergoes photolysis, releasing Br atoms that form BrO by reacting with ozone. This photochemical heterogeneous production of reactive halogen species is highly accelerated in a frozen solution (i.e., brine layers and ice-grain boundary) due to the freeze concentration effects of multiple solutes (Kim et al., 2019b; Kim et al., 2016). This phenomenon occurs because ice has the property of being selectively intolerant to impurities (Robinson et al., 2006). These findings indicate that chemical processes occurring in icy areas, particularly first-year sea ice, can facilitate the release of reactive halogen species, including BrO. Thus, the prolonged air mass exposure over the first-year ice zone can induce atmospheric BrO enrichment, which thereby strengthens the DMS oxidation capacity as observed for WAP and EAP zones.

4.3. DMS-induced particle formation

The measured CN_{10-25} from the WAP and EAP was 2.4- and 1.8-fold greater than that of the AOO, respectively (Fig. 4f). These results indicate that new particles, possibly derived from DMS and other gaseous precursors, were more intensively formed when the air masses passed through ice-related zones. Particularly, the moderate balance between the key aerosol precursor (i.e., DMS) and efficient oxidant (i.e., BrO), which were actively released from the first-year ice zones, can provide favorable conditions to trigger the oxidation of DMS and form new DMS-induced particles. The 8-year (2009–2016) field observations of the physical properties of the aerosol particles at the same observation site also showed clear differences in new particle formation events depending on the origin of air masses (Kim et al., 2019a; Kim et al., 2017). For example, the number concentrations of nano-size particles (2.5–10 nm in diameter) from air masses originating from the western part of Antarctic Peninsula (~400 cm^{-3}) were higher than those originating from the eastern (~340 cm^{-3}) and northern Antarctic Peninsula (i.e., pelagic Southern Ocean; ~20 cm^{-3}) (Kim et al., 2017). Moreover, more than half of the new particle formation events with higher particle formation rates (> 3 cm^{-3} s^{-1}) were observed when the air mass originated from the western part of the Antarctic Peninsula (Kim et al., 2019a). Recent shipboard measurements of the chemical properties of submicron aerosol particles and onboard aerosol generation experiments in the Southern Ocean also support that aerosol particles originate from sympagic areas predominated by secondary organic

aerosols, including nss-SO_4^{2-}, MSA, and N compounds. In contrast, the aerosol particles from the pelagic ocean were enriched with primary aerosols, including lipids, sugars, and sea salt (Dall'Osto et al., 2017b; Decesari et al., 2020; Rinaldi et al., 2020).

Although the atmospheric DMS mixing ratios in the EAP were approximately two-fold lower than those in the WAP and AOO, the $CN_{10–25}$ in the EAP was two-fold higher than that in the AOO and only 35% lower than that in the WAP (Fig. 4f). This indicates that a fraction of the newly formed particles from the EAP and WAP could possibly result from gaseous precursors other than DMS. Among the aerosol precursors, iodine oxide particles (IOP) are known to significantly increase the formation of new particles in the polar regions (Allan et al., 2015; Baccarini et al., 2020; Roscoe et al., 2015). Results from the CAM-Chem model showed that the highest monthly mean surface IO mixing ratios were in the EAP (0.16 ± 0.08 pptv), followed by the WAP (0.10 ± 0.04 pptv) and AOO (0.08 ± 0.03 pptv) (Figs. 3e and S5b). Although our field observations did not account for the contribution of other aerosol precursors (e.g., N-compounds) to particle formation and growth, we expect significant IOP formation in the EAP region.

5. Conclusions and implications

In this study, we provided new insights into the role of DMS in forming aerosols in coastal Antarctica based on an analysis of source region-dependent emissions and oxidation of DMS. Our results indicate the following: (1) Atmospheric DMS levels could be modulated by the taxonomic compositions of pelagic phytoplankton and ice algal blooms. (2) Higher DMS oxidation capacity driven by BrO could intensify DMS-derived new particle formation in the Antarctic Peninsula. (3) Biological and chemical processes actively occurring in the first-year ice zone could enhance DMS-derived particle formation by supplying both key aerosol precursors and efficient oxidants into the Antarctic boundary layer. Consequently, these results provide a process-level understanding of DMS-induced particle formation depending on source regions and suggest that future changes in sea ice properties could have a significant impact on sulfurous particle formation in the Antarctic Peninsula.

The Antarctic Peninsula, especially the western portion, has been warming faster than the rest of the planet since the 20th century (Sato et al., 2021; Tuckett et al., 2019). A change in the sea ice coverage and its properties (i.e., decline in the total extent, reduced sea ice season duration, and shift from multi-year sea ice to first-year sea ice) can affect the formation of DMS-derived particles in the Antarctic Peninsula; the magnitude and direction of these effects may vary in different regions. Thus, a regional-scale understanding of the DMS-induced particle formation in concert with comprehensive investigations of multiple environmental variables in Antarctica is imperative to improve climate change predictions. Emissions of biogenic volatile organic compounds and their reaction with atmospheric oxidants are important in aerosol-formation processes as well as to radiative climate forcing (Brooks and Thornton, 2018; Piller-Little and Guzman, 2018). Hence, long-term observations of gas- and aqueous-phase aerosol precursors, reactive halogen species, and the physiochemical properties of aerosol particles are necessary to provide a better understanding of ocean–cryosphere–atmosphere interactions and their association with climate feedbacks in fragile Antarctica.

CRediT authorship contribution statement

Eunho Jang: Formal analysis, Writing – original draft, Visualization. **Ki-Tae Park:** Conceptualization, Writing – original draft, Writing – review & editing, Supervision. **Young Jun Yoon:** Conceptualization, Writing – review & editing. **Kitae Kim:** Conceptualization, Writing – review & editing. **Yeontae Gim:** Investigation. **Hyun Young Chung:** Investigation. **Kitack Lee:** Conceptualization, Writing – review & editing. **Jinhee Choi:** Investigation. **Jiyeon Park:** Conceptualization, Writing – review & editing. **Sang-Jong Park:** Resources, Writing – review & editing. **Ja-Ho Koo:** Conceptualization, Writing – review & editing. **Rafael P. Fernandez:** Resources, Writing – review & editing. **Alfonso Saiz-Lopez:** Resources, Writing – review & editing.

Declaration of competing interest

The authors declare that they have no known competing financial interests or personal relationships that could have appeared to influence the work reported in this paper.

Acknowledgments

We thank the overwintering staff for assisting us in maintaining the aerosol equipment at the King Sejong station. This study was supported by the KOPRI project (PE21030 and PE21120). KL was supported by the National Research Foundation of Korea (NRF-2021R1A2C3008748). The datasets for atmospheric DMS, its oxidative products, and aerosol size distribution are available at the Korea Polar Data Center (https://dx.doi.org/doi:10.22663/KOPRI-KPDC-00001657.4). The sea ice data can be downloaded from the NSIDC website (https://nsidc.org/data/G02135/versions/3). The MODIS-Aqua products can be downloaded from the NASA Ocean Color website (https://oceandata.sci.gsfc.nasa.gov/MODIS-Aqua/). MIMOC is available at https://www.pmel.noaa.gov/mimoc/. The PHYSAT products can be accessed from the PHYSAT website (https://log.cnrs.fr/Physat-332). The code for the CAM-Chem model is available at https://www2.acom.ucar.edu/gcm/cam-chem.

Appendix A. Supplementary data

Supplementary data to this article can be found online at https://doi.org/10.1016/j.scitotenv.2021.150002.

References

Allan, J.D., Williams, P.I., Najera, J., Whitehead, J.D., Flynn, M.J., Taylor, J.W., Liu, D., Darbyshire, E., Carpenter, L.J., Chance, R., Andrews, S.J., Hackenberg, S.C., McFiggans, G., 2015. Iodine observed in new particle formation events in the Arctic atmosphere during ACCACIA. Atmos. Chem. Phys. 15, 5599–5609. https://doi.org/10.5194/acp-15-5599-2015.

Alvain, S., Moulin, C., Dandonneau, Y., Loisel, H., 2008. Seasonal distribution and succession of dominant phytoplankton groups in the global ocean: a satellite view. Glob. Biogeochem. Cycl. 22, GB3001. https://doi.org/10.1029/2007GB003154.

Arrigo, K.R., Mills, M.M., Kropuenske, L.R., van Dijken, G.L., Alderkamp, A.-C., Robinson, D.H., 2010. Photophysiology in two major Southern Ocean phytoplankton taxa: photosynthesis and growth of Phaeocystis antarctica and Fragilariopsis cylindrus under different irradiance levels. Integ. Comp. Biol. 50, 950–966. https://doi.org/10.1093/icb/icq021.

Asmi, E., Neitola, K., Teinilä, K., Rodriguez, E., Virkkula, A., Backman, J., Bloss, M., Jokela, J., Lihavainen, H., de Leeuw, G., Paatero, J., Aaltonen, V., Mei, M., Gambarte, G., Copes, G., Albertini, M., Fogwill, G.P., Ferrara, J., Barlasina, M.E., Sánchez, R., 2018. Primary sources control the variability of aerosol optical properties in the Antarctic peninsula. Tellus B 70, 1–16. https://doi.org/10.1080/16000889.2017.1414571.

Baccarini, A., Karlsson, L., Dommen, J., Duplessis, P., Vüllers, J., Brooks, I.M., Saiz-Lopez, A., Salter, M., Tjernström, M., Baltensperger, U., Zieger, P., Schmale, J., 2020. Frequent new particle formation over the high Arctic pack ice by enhanced iodine emissions. Nat. Commun. 11, 4924. https://doi.org/10.1038/s41467-020-18551-0.

Barnes, I., Hjorth, J., Mihalopoulos, N., 2006. Dimethyl sulfide and dimethyl sulfoxide and their oxidation in the atmosphere. Chem. Rev. 106, 940–975. https://doi.org/10.1021/cr020529.

Berresheim, H., Huey, J.W., Thorn, R.P., Eisele, F.L., Tanner, D.J., Jefferson, A., 1998. Measurements of dimethyl sulfide, dimethyl sulfoxide, dimethyl sulfone, and aerosol ions at Palmer Station, Antarctica. J. Geophys. Res.-Atmos. 103, 1629–1637. https://doi.org/10.1029/97JD00695.

Boucher, O., Lohmann, U., 1995. The sulfate-CCN-cloud albedo effect. Tellus B 47, 281–300. https://doi.org/10.3402/tellusb.v47i3.16048.

Boucher, O., Moulin, C., Belviso, S., Aumont, O., Bopp, L., Cosme, E., von Kuhlmann, R., Lawrence, M.G., Pham, M., Reddy, M.S., Sciare, J., Venkataraman, C., 2003. DMS atmospheric concentrations and sulphate aerosol indirect radiative forcing: a sensitivity study to the DMS source representation and oxidation. Atmos. Chem. Phys. 3, 49–65. https://doi.org/10.5194/acp-3-49-2003.

Brean, J., Dall'Osto, M., Simó, R., Shi, Z., Beddows, D.C.S., Harrison, R.M., 2021. Open Ocean and coastral new particle formation from sulfuric acid and amines around the Antarctic peninsula. Nat. Geosci. 14, 383–388. https://doi.org/10.1038/s41561-021-00751-y.

Breider, T.J., Chipperfield, M.P., Richards, N.A.D., Carslaw, K.S., Mann, G.W., Spracklen, D.V., 2010. Impact of BrO on dimethylsulfide in the remote marine boundary layer. Geophys. Res. Lett. 37, L02807. https://doi.org/10.1029/2009GL040868.

Brooks, S.D., Thornton, D.C.O., 2018. Marine aerosols and clouds. Annu. Rev. Mar. Sci. 10, 289–313. https://doi.org/10.1146/annurev-marine-121916-063148.

Browse, J., Carslaw, K.S., Mann, G.W., Birch, C.E., Arnold, S.R., Leck, C., 2014. The complex response of Arctic aerosol to sea-ice retreat. Atmos. Chem. Phys. 14, 7543–7557. https://doi.org/10.5194/acp-14-7543-2014.

Carslaw, K.S., Lee, L.A., Reddington, C.L., Pringle, K.J., Rap, A., Forster, P.M., Mann, G.W., Spracklen, D.V., Woodhouse, M.T., Regayre, L.A., Pierce, J.R., 2013. Large contribution of natural aerosols to uncertainty in indirect forcing. Nature 503, 67–71. https://doi.org/10.1038/nature12674.

Chang, R.Y.-W., Sjostedt, S.J., Pierce, J.R., Papakyriakou, T.N., Scarratt, M.G., Michaud, S., Levasseur, M., Leaitch, W.R., Abbatt, J.P.D., 2011. Relating atmospheric and oceanic DMS levels to particle nucleation events in the Canadian Arctic. J. Geophys. Res.-Atmos. 116, D00S03. https://doi.org/10.1029/2011JD015926.

Charlson, R.J., Lovelock, J.E., Andreae, M.O., Warren, S.G., 1987. Oceanic phytoplankton, atmospheric Sulphur, cloud albedo and climate. Nature 326, 655–661. https://doi.org/10.1038/326655a0.

Chen, Q., Sherwen, T., Evans, M., Alexander, B., 2018. DMS oxidation and sulfur aerosol formation in the marine troposphere: a focus on reactive halogen and multiphase chemistry. Atmos. Chem. Phys. 18, 13617–13637. https://doi.org/10.5194/acp-18-13617-2018.

Choi, J.H., Jang, E., Yoon, Y.J., Park, J.Y., Kim, T.-W., Becagli, S., Caiazzo, L., Cappelletti, D., Krejci, R., Eleftheriadis, K., Park, K.-T., Jang, K.S., 2019. Influence of biogenic organics on the chemical composition of Arctic aerosols. Glob. Biogeochem. Cycl. 33, 1238–1250. https://doi.org/10.1029/2019GB006226.

Curran, M.A.J., Jones, G.B., 2000. Dimethyl sulfide in the Southern Ocean: seasonality and flux. J. Geophys. Res.-Atmos. 105, 20451–20459. https://doi.org/10.1029/2000JD900176.

Dall'Osto, M., Beddows, D.C.S., Tunved, P., Krejci, R., Ström, J., Hansson, H.-C., Yoon, Y.J., Park, K.-T., Becagli, S., Udisti, R., Onasch, T., O'dowd C.D. Marrison R.M., Simó R., 2017. Arctic Sea ice melt leads to atmospheric new particle formation. Sci. Rep. 7, 3318. https://doi.org/10.1038/s41598-017-03328-1.

Dall'Osto, M., Ovadnevaite, J., Paglione, M., Beddows, D.C.S., Ceburnis, D., Cree, C., Cortés, P., Zamanillo, M., Nunes, S.O., Pérez, G.L., Ortega-Retuerta, E., Emelianov, M., Vaque, D., Marrasé, C., Estrada, M., Sala, M.M., Vidal, M., Fitzsimons, M.F., Beale, R., Airs, R., Rinaldi, M., Decesari, S., Facchini, M.C., Harrison, R.M., O'Dowd, C., Simó, R., 2017b. Antarctic Sea ice region as a source of biogenic organic nitrogen in aerosols. Sci. Rep. 7, 6047. https://doi.org/10.1038/s41598-017-06188-x.

Decesari, S., Paglione, M., Rinaldi, M., Dall'Osto, M., Simó, R., Zanca, N., Volpi, F., Facchini, M.C., Hoffmann, T., Götz, S., Kampf, C.J., O'Dowd, C., Ceburnis, D., Ovadnevaite, J., Tagliavini, E., 2020. Shipborne measurements of Antarctic submicron organic aerosols: an NMR perspective linking multiple sources and bioregions. Atmos. Chem. Phys. 20, 4193–4207. https://doi.org/10.5194/acp-20-4193-2020.

Fernandez, R.P., Carmona-Balea, A., Cuevas, C.A., Barrera, J.A., Kinnison, D.E., Lamarque, J.-F., Blaszczak-Boxe, C., Kim, K., Choi, W., Hay, T., Blechschmidt, A.-M., Schönhardt, A., Burrows, J.P., Saiz-Lopez, A., 2019. Modeling the sources and chemistry of polar tropospheric halogens (Cl, br, and I) using the CAM-chem global chemistry-climate model. J. Adv. Model. Earth Syst. 11, 2259–2289. https://doi.org/10.1029/2019MS001655.

Galí, M., Devred, E., Levasseur, M., Royer, S.-J., Babin, M., 2015. A remote sensing algorithm for planktonic dimethylsulfoniopropionate (DMSP) and an analysis of global patterns. Remote Sens. Environ. 171, 171–184. https://doi.org/10.1016/j.rse.2015.10.012.

von Glasow, R., Crutzen, P.J., 2004. Model study of multiphase DMS oxidation with a focus on halogens. Atmos. Chem. Phys. 4, 589–608. https://doi.org/10.5194/acp-4-589-2004.

Guzman, M.I., Athalye, R.R., Rodriguez, M., 2012. Concentration effects and ion properties controlling the fractionation of halides during aerosol formation. J. Phys. Chem. A 116, 5428–5435. https://doi.org/10.1021/jp3011316.

Haywood, J.M., Boucher, O., 2000. Estimates of the direct and indirect radiative forcing due to tropospheric aerosols: a review. Rev. Geophys. 38, 513–543. https://doi.org/10.1029/1999RG000078.

Hodshire, A.L., Palm, B.B., Alexander, M.L., Bian, Q., Campuzano-Jost, P., Cross, E.S., Day, D.A., de Sá, S.S., Guenther, A.B., Hansel, A., Hunter, J.F., Jud, W., Karl, T., Kim, S., Kroll, J.H., Park, J.-H., Peng, Z., Seco, R., Smith, J.N., Jimenez, J.L., Pierce, J.R., 2018. Constraining nucleation, condensation, and chemistry in oxidation flow reactors using size-distribution measurements and aerosol microphysical modeling. Atmos. Chem. Phys. 18, 12433–12460. https://doi.org/10.5194/acp-18-12433-2018.

Holmes, N., 2007. A review of particle formation events and growth in the atmosphere in the various environments and discussion of mechanistic implications. Atmos. Environ. 41, 2183–2201. https://doi.org/10.1016/j.atmosenv.2006.10.058.

Hong, S.-B., Yoon, Y.J., Becagli, S., Gim, Y., Chambers, S.D., Park, K.-T., Park, S.-J., Traversi, R., Severi, M., Vitale, V., Kim, J.-H., Jang, E., Crawford, J., Griffiths, A.D., 2020. Seasonality of aerosol chemical composition at king Sejong Station (Antarctic Peninsula) in 2013. Atmos. Environ. 223, 117185. https://doi.org/10.1016/j.atmosenv.2019.117185.

Hughes, C., Johnson, M., von Glasow, R., Chance, R., Atkinson, H., Souster, T., Lee, G.A., Clarke, A., Meredith, M., Venables, H.J., Turner, S.M., Malin, G., Liss, P.S., 2012. Climate-induced change in biogenic bromine emissions from the Antarctic marine biosphere. Glob. Biogeochem. Cycl. 26, GB3019. https://doi.org/10.1029/2012GB004295.

Jang, S., Park, K.-T., Lee, K., Suh, Y.-S., 2016. An analytical system enabling consistent and long-term measurement of atmospheric dimethyl sulfide. Atmos. Environ. 134, 217–223. https://doi.org/10.1016/j.atmosenv.2016.03.041.

Jang, E., Park, K.-T., Yoon, Y.J., Kim, T.-W., Hong, S.-B., Becagli, S., Traversi, R., Kim, J., Gim, Y., 2019. New particle formation events observed at the king Sejong Station, Antarctic peninsula – part 2: link with the oceanic biological activities. Atmos. Chem. Phys. 19, 7595–7608. https://doi.org/10.5194/acp-19-7595-2019.

Jang, S., Park, K.-T., Lee, K., Yoon, Y.J., Kim, K., Chung, H.Y., Jang, E., Becagli, S., Lee, B.Y., Traversi, R., Eleftheriadis, K., Krejci, R., Hermansen, O., 2021. Large seasonal and interannual variations of biogenic sulfur compounds in the Arctic atmosphere (Svalbard; 78.9° N, 11.9° E). Atmos. Chem. Phys. 21, 9761–9777. https://doi.org/10.5194/acp-21-9761-2021.

Jarníková, T., Dacy, J., Lizotte, M., Levasseur, M., Tortell, P., 2018. The distribution of methylated sulfur compounds, DMS and DMSP, in Canadian subarctic and artic marine waters during summer 2015. Biogeosciences 15, 2449–2465. https://doi.org/10.5194/bg-15-2449-2018.

Jokinen, T., Sipilä, M., Kontkanen, J., Vakkari, V., Tisler, P., Duplissy, E.-M., Junninen, H., Kangasluoma, J., Manninen, H.E., Petäjä, T., Kulmala, M., Worsnop, D.R., Kirkby, J., Virkkula, A., Kerminen, V.-M., 2018. Ion-induced sulfuric acid-ammonia nucleation drives particle formation in coastal Antarctica. Sci. Adv. 4, eaat9744. https://doi.org/10.1126/sciadv.aat9744.

Keene, W.C., Pszenny, A.A.P., Galloway, J.N., Hawley, M.E., 1989. Sea-salt corrections and interpretation of constituent ratios in marine precipitation. J. Geophys. Res.-Atmos. 91, 6647–6658. https://doi.org/10.1029/JD091iD06p06647.

Keller, M.D., Bellows, W.K., Guillard, R.L., 1989. Dimethyl sulfideproduction in marine phytoplankton. In: Saltzman, E.S., Cooper, W.J. (Eds.), Biogenic Sulfur in the Environment. American Chemical Society, Washington, DC, pp. 167–182.

Kerminen, V.-M., Chen, X., Vakkari, V., Petäjä, T., Kulmala, M., Bianchi, F., 2018. Atmospheric new particle formation and growth: review of field observations. Environ. Res. Lett. 13, 103003. https://doi.org/10.1088/1748-9326/aadf3c.

Kim, K., Yabushita, A., Okumura, M., Saiz-Lopez, A., Cuevas, C.A., Blaszczak-Boxe, C.S., Min, D.W., Yoon, H.I., Choi, W., 2016. Production of molecular iodine and tri-iodide in the frozen solution of iodide: implication for polar atmosphere. Environ. Sci. Technol. 50, 1280–1287. https://doi.org/10.1021/acs.est.5b05148.

Kim, J., Yoon, Y.J., Gim, Y., Kang, H.J., Choi, J.H., Park, K.-T., Lee, B.Y., 2017. Seasonal variations in physical characteristics of aerosol particles at the king Sejong Station, Antarctic peninsula. Atmos. Chem. Phys. 17, 12985–12999. https://doi.org/10.5194/acp-17-12985-2017.

Kim, J., Yoon, Y.J., Gim, Y., Choi, J.H., Kang, H.J., Park, K.-T., Park, J., Lee, B.Y., 2019a. New particle formation events observed at king Sejong Station, Antarctic peninsula – part 1: physical characteristics and contribution to cloud condensation nuclei. Atmos. Chem. Phys. 19, 7583–7594. https://doi.org/10.5194/acp-19-7583-2019.

Kim, K., Menacherry, S.P.M., Kim, J., Chung, H.Y., Jeong, D., Saiz-Lopez, A., Choi, W., 2019b. Simultaneous and synergic production of bioavailable iron and reactive iodine species in ice. Environ. Sci. Technol. 53, 7355–7362. https://doi.org/10.1021/acs.est.8b06659.

Kirst, G.O., Thiel, C., Wolff, H., Nothnagel, J., Wanzek, M., Ulmke, R., 1991. Dimethylsulfoniopropionate (DMSP) in icealgae and its possible biological role. Mar. Chem. 35, 381–388. https://doi.org/10.1016/S0304-4203(09)90030-5.

Koga, S., Nomura, D., Wada, M., 2014. Variation of dimethylsulfide mixing ratio over the Southern Ocean from 36°S to 70°S. Polar Sci. 8, 306–313. https://doi.org/10.1016/j.polar.2014.04.002.

Lachlan-Cope, T., Beddows, D.C.S., Brough, N., Jones, A.E., Harrison, R.M., Lupi, A., Yoon, Y.J., Virkkula, A., Dall'Osto, M., 2020. On the annual variability of Antarctic aerosol size distributions at Halley Research Station. Atmos. Chem. Phys. 20, 4461–4476. https://doi.org/10.5194/acp-20-4461-2020.

Lana, A., Bell, T.G., Simó, R., Vallina, S.M., Ballabrera-Poy, J., Kettle, A.J., Dachs, J., Bopp, L., Saltzman, E.S., Stefels, J., Johnson, J.E., Liss, P.S., 2011. An updated climatology of surface dimethlysulfide concentrations and emission fluxes in the global ocean. Glob. Biogeochem. Cycl. 25, GB1004. https://doi.org/10.1029/2010GB003850.

Leaitch, W.R., Sharma, S., Huang, L., Toom-Sauntry, D., Chivulescu, A., Macdonald, A.M., von Salzen, K., Pierce, J.R., Bertram, A.K., Schroder, J.C., Shantz, N.C., Chang, R.Y.-W., Norman, A.-L., 2013. Dimethyl sulfide control of the clean summertime Arctic aerosol and cloud. Elementa (Wash. D.C.) 1, 000017. https://doi.org/10.12952/journal.elementa.000017.

Levasseur, M., 2013. Impact of Arctic meltdown on the microbial cycling of sulphur. Nat. Geosci. 6, 691–700. https://doi.org/10.1038/NGEO1910.

Lieb-Lappen, R.M., Obbard, R.W., 2015. The role of blowing snow in the activation of bromine over first-year Antarctic Sea ice. Atmos. Chem. Phys. 15, 7537–7545. https://doi.org/10.5194/acp-15-7537-2015.

Mahajan, A.S., Fadnavis, S., Thomas, M.A., Pozzoli, L., Gupta, S., Royer, S.-J., Saiz-Lopez, A., Simó, R., 2015. Quantifying the impacts of an updated global dimethyl sulfide climatology on cloud microphyics and aerosol radiative forcing. J. Geophys. Res. Atmos. 120, 2524–2536. https://doi.org/10.1002/2014JD022687.

Mungall, E.L., Croft, B., Lizotte, M., Thomas, J.L., Murphy, J.G., Levasseur, M., Martin, R.V., Wentzell, J.J.B., Liggio, J., Abbatt, P.D., 2016. Dimethyl sulfide in the summertime Arctic atmosphere: measurements and source sensitivity simulations. Atmos. Chem. Phys. 16, 6665–6680. https://doi.org/10.5194/acp-16-6665-2016.

O'Dowd, C.D., Facchini, M.C., Cavalli, F., Ceburnis, D., Mircea, M., Decesari, S., Fuzzi, S., Yoon, Y.J., Putaud, J.-P., 2004. Biogenically driven organic contribution to marine aerosol. Nature 431, 676–680. https://doi.org/10.1038/nature02959.

Park, K.-T., Lee, K., Yoon, Y.-J., Lee, H.-W., Kim, H.-C., Lee, B.-Y., Hermansen, O., Kim, T.-W., Helmén, K., 2013. Linking atmospheric dimethyl sulfide and the Arctic Ocean spring bloom. Geophys. Res. Lett. 40, 1–6. https://doi.org/10.1029/2012GL054560.

Park, K.-T., Lee, K., Shin, K., Yang, E.-J., Hyun, B., Kim, J.-M., Noh, J.H., Kim, M., Kong, B., Choi, D.H., Choi, S.-J., Jang, P.-G., Jeong, H.J., 2014. Direct linkage between dimethyl sulfide production and microzooplankton grazing, resulting from prey composition change under high partial pressure of carbon dioxide conditions. Environ. Sci. Technol. 48, 4750–4756. https://doi.org/10.1021/es403351h.

Park, K.-T., Jang, S., Lee, K., Yoon, Y.J., Kim, M.-S., Park, K., Cho, H.-J., Kang, J.-H., Udisti, R., Lee, B.-Y., Shin, K.-H., 2017. Observational evidence for the formation of DMS-derived aerosols during Arctic phytoplankton blooms. Atmos. Chem. Phys. 17, 9665–9675. https://doi.org/10.5194/acp-17-9665-2017.

Park, K.-T., Lee, K., Kim, T.-W., Yoon, Y.J., Jang, E.-H., Jang, S., Lee, B.-Y., Hermansen, O., 2018. Atmospheric DMS in the Arctic Ocean and its relation to phytoplankton biomass. Glob. Biogeochem. Cycl. 32, 351–359. https://doi.org/10.1002/2017GB005805.

Park, J., Dall'Osto, M., Park, K., Gim, Y., Kang, H.J., Jang, E., Park, K.-T., Park, M., Yum, S.S., Jung, J., Lee, B.Y., Yoon, Y.J., 2020. Shipborne observations reveal contrasting Arctic marine, Arctic terrestrial and Pacific marine aerosol properties. Atmos. Chem. Phys. 20, 5573–5590. https://doi.org/10.5194/acp-20-5573-2020.

Park, K.-T., Yoon, Y.J., Lee, K., Tunved, P., Krejci, R., Ström, J., Jang, E., Kang, H.J., Jang, S., Park, J., Lee, B.Y., Traversi, R., Becagli, S., Hermansen, O., 2021. Dimethyl sulfide-induced increase in cloud condensation nuclei in the Arctic atmosphere. Glob. Biogeochem. Cycl. 35. https://doi.org/10.1029/2021GB006969 (e2021GB006969).

Piller-Little, E.A., Guzman, M.I., 2018. An overview of dynamic heterogeneous oxidations in the troposphere. Environments. 5, 104. https://doi.org/10.3390/environments5090104.

Piller-Little, E.A., Guzman, M.I., Rodriguez, J.M., 2013. Conversion of iodide to hypoiodous acid and iodine in aqueous microdroplets exposed to ozone. Environ. Sci. Technol. 47, 10971–10979. https://doi.org/10.1021/es401700h.

Pratt, K.A., 2019. Tropospheric halogen photochemistry in the rapidly changing Arctic. Trends Chem. 1, 545–548. https://doi.org/10.1016/j.trechm.2019.06.001.

Read, K.A., Lewis, A.C., Bauguitte, S., Rankin, A.M., Salmon, R.A., Wolff, E.W., Saiz-Lopez, A., Bloss, W.J., Heard, D.E., Lee, J.D., Plane, J.M.C., 2008. DMS and MSA measurements in the Antarctic boundary layer: impact of BrO on MSA production. Atmos. Chem. Phys. 8, 2985–2997. https://doi.org/10.5194/acp-8-2985-2008.

Rinaldi, M., Paglione, M., Decesari, S., Harrison, R.M., Beddows, D.C.S., Ovadnevaite, J., Ceburnis, D., O'Dowd, C., Simó, R., Dall'Osto, M., 2020. Contribution of water-soluble organic matter from multiple marine geographic eco-regions to aerosols around Antarctica. Environ. Sci. Technol. 54, 7807–7817. https://doi.org/10.1021/acs.est.0c00695.

Robinson, C., Boxe, C.S., Guzman, M.I., Golussi, A.J., Hoffmann, M.R., 2006. Acidity of frozen electrolyte solutions. J. Phys. Chem. B 110, 7613–7616. https://doi.org/10.1021/jp061169n.

Rolph, G., Stein, A., Stunder, B., 2017. Real-time Environmental Applications and Display sYstem: READY. Environ. Modell. Softw. 95, 210–228. https://doi.org/10.1016/j.envsoft.2017.06.025.

Roscoe, H.K., Jones, A.E., Brough, N., Weller, R., Saiz-Lopez, A., Mahajan, A.S., Schoenhardt, A., Burrows, J., Fleming, Z.L., 2015. Particles and iodine compounds in coastal Antarctica. J. Geophys. Res. Atmos. 120, 7144–7156. https://doi.org/10.1002/2015JD023301.

Saiz-Lopez, A., von Glasow, R., 2012. Reactive halogen chemistry in the troposphere. Chem. Soc. Rev. 41, 6448–6472. https://doi.org/10.1039/c2cs35208g.

Saiz-Lopez, A., Mahajan, A.S., Salmon, R.A., Bauguitte, S.J.-B., Jones, A.E., Roscoe, H.K., Plane, J.M.C., 2007. Boundary layer halogens in coastal Antarctica. Science 317, 348–351. https://doi.org/10.1126/science.1141408.

Saiz-Lopez, A., Plane, J.M.C., Mahajan, A.S., Anderson, P.S., Bauguitte, S.J.-B., Jones, A.E., Roscoe, H.K., Salmon, R.A., Bloss, W.J., Lee, J.D., Heard, D.E., 2008. On the vertical distribution of boundary layer halogens over coastal Antarctica: implications for O3, HOx, NOx and the hg lifetime. Atmos. Chem. Phys. 8, 887–900. https://doi.org/10.5194/acp-8-887-2008.

Sanchez, K.J., Chen, C.-L., Russell, L.M., Betha, R., Liu, J., Price, D.J., Massoli, P., Ziemba, L.D., Crosbie, E.C., Moore, R.H., Müller, M., Schiller, S.A., Wisthaler, A., Lee, A.K.Y., Quinn, P.K., Bates, T.S., Porter, J., Bell, T.G., Saltzman, E.S., Vaillancourt, R.D., Behrenfeld, M.J., 2018. Substantial seasonal contribution of observed biogenic sulfate particles to cloud condensation nuclei. Sci. Rep. 8, 3235. https://doi.org/10.1038/s41598-018-21590-9.

Sato, K., Inoue, J., Simmonds, I., Rudeva, I., 2021. Antarctic peninsula warm winters influenced by Tasman Sea temperatures. Nat. Commun. 12, 1497. https://doi.org/10.1038/s41467-021-21773-5.

Sharma, S., Barrie, L.A., Plummer, D., McConnell, J.C., Brickell, P.C., Levasseur, M., Gosselin, M., Bates, T.S., 1999. Flux estimation of oceanic dimethyl sulfide around North America. J. Geophys. Res.-Atmos. 104, 21327–21342. https://doi.org/10.1029/1999JD900207.

Simó, R., 2001. Production of atmospheric sulfur by oceanic plankton: biogeochemical, ecological and evolutionary links. Trends Ecol. Evol. 16, 287–294. https://doi.org/10.1016/S0169-5347(01)02152-8.

Simpson, W.R., von Glasow, R., Riedel, K., Anderson, P., Ariya, P., Bottenheim, J., Burrows, J., Carpenter, L.J., Frieß, U., Goodsite, M.E., Heard, D., Hutterli, M., Jacobi, H.-W., Kaleschke, L., Neff, B., Plane, J., Platt, U., Richter, A., Roscoe, H., Sander, R., Shepson, P., Sodeau, J., Steffen, A., Wagner, T., Wolff, E., 2007. Halogens and their role in polar boundary-layer ozone depletion. Atmos. Chem. Phys. 7, 4375–4418. https://doi.org/10.5194/acp-7-4375-2007.

Stefels, J., Steinke, M., Turner, S., Malin, G., Belviso, S., 2007. Environmental constraints on the production and removal of the climatically active gas dimethylsulphide (DMS) and implications for ecosystem modelling. Biogeochemistry 83, 245–275. https://doi.org/10.1007/s10533-007-9091-5.

Stein, A.F., Draxler, R.R., Rolph, G.D., Stunder, B.J.B., Cohen, M.D., Ngan, F., 2015. NOAA's HYSPLIT atmospheric transport and dispersion modeling system. B. Am. Meteorol. Soc. 96, 2059–2077. https://doi.org/10.1175/BAMS-D-14-00110.1.

Strom, S., Wolfe, G., Slajer, A., Lambert, S., Clough, J., 2003. Chemical defense in the microplankton II: inhibition of protist feeding by ß-dimethylsulfoniopropionate (DMSP). Limnol. Oceanog. 48, 230–237. https://doi.org/10.4319/lo.2003.48.1.0230.

Strong, C., Rigor, I.G., 2013. Arctic marginal ice zone trending wider in summer and narrower in winter. Geophys. Res. Lett. 40, 4864–4868. https://doi.org/10.1002/grl.50928.

Sunda, W., Kieber, D.J., Kiene, R.P., Huntsman, S., 2002. An antioxidant function for DMSP and DMS in marine algae. Nature 418, 317–320. https://doi.org/10.1038/nature00851.

Trevena, A.J., Jones, G.B., 2006. Dimethylsulphide and dimethylsulphoniopropionate in Antarctic Sea ice and their release during sea ice melting. Mar. Chem. 98, 210–222. https://doi.org/10.1016/j.marchem.2005.09.005.

Tuckett, P.A., Ely, J.C., Sole, A.J., Livingstone, S.J., Davison, B.J., Melchior van Wessem, J., Howard, J., 2019. Rapid accelerations of Antarctic peninsula outlet glaciers driven by surface melt. Nat. Commun. 10, 4311. https://doi.org/10.1038/s41467-019-12039-2.

Veres, P.R., Neuman, J.A., Bertram, T.H., Assaf, E., Wolfe, G.M., Williamson, C.J., Weinzierl, B., Tilmes, S., Thompson, C.R., Thames, A.B., Schroder, J.C., Saiz-Lopez, A., Rollins, A.W., Roberts, J.M., Price, D., Peischl, J., Kupc, A., Kjaergaard, H.G., Kinnison, D., Jimenez, J.L., Jernigan, C.M., Hornbrook, R.S., Hills, A., Dollner, M., Day, D.A., Cuevas, C.A., Campuzano-Jost, P., Burkholder, J., Bui, T.P., Brune, W.H., Brown, S.S., Brock, C.A., Bourgeois, I., Blake, D.R., Apel, E.C., Ryerson, T.B., 2020. Global airborne sampling reveals a previously unobserved dimethyl sulfide oxidation mechanism in the marine atmosphere. Proc. Natl. Acad. Sci. U. S. A. 117, 4505–4510. https://doi.org/10.1073/pnas.1919344117.

Yan, J., Jung, J., Lin, Q., Zhang, M., Xu, S., Zhao, S., 2020a. Effect of sea ice retreat on marine aerosol emissions in the Southern Ocean, Antarctica. Sci. Total Environ. 745, 140773. https://doi.org/10.1016/j.scitotenv.2020.140773.

Yan, J., Zhang, M., Jung, J., Lin, Q., Zhao, S., Xu, S., Chen, L., 2020b. Influence on the conversion of DMS to MSA and SO42- in the Southern Ocean, Antarctica. Atmos. Environ. 233, 117611. https://doi.org/10.1016/j.atmosenv.2020.117611.

Yang, X., Pyle, J.A., Cox, R.A., 2008. Sea salt aerosol production and bromine release: role of snow on sea ice. Geophys. Res. Lett. 35, 16. https://doi.org/10.1029/2008GL034536.